Asian Journal of Chemistry; Vol. 29, No. 4 (2017), 917-922

ASIAN JOURNAL OF CHEMISTRY

https://doi.org/10.14233/ajchem.2017.20370

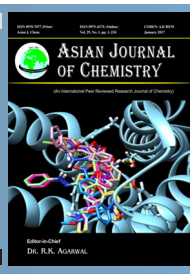

Electrodeposition of Zn-Graphite Oxide Nanocomposite Coatings on Stainless Steel from Sulfate Bath, its Surface Morphological and Corrosion Protection Studies

GANESHA ACHARY[1,*], D.A. PRATHIMA MATHIAS[1] and Y. ARTHOBA NAYAKA[2]

[1]Department of P.G. Studies in Chemistry, I.D.S.G. Government College, Chikmagalur-577 101, India
[2]School of Chemical Sciences, Kuvempu University, Shankaraghatta-577 451, India

*Corresponding author: E-mail: gani_papu@yahoo.co.in

Received: 24 October 2016; *Accepted*: 13 January 2017; *Published online*: 31 January 2017; AJC-18273

Thin films of Zn-GO nanocomposites were prepared by electrodeposition in sulfate bath solution with different concentration of dispersed graphite oxide (GO) colloid. Various bath parameters were optimized to get the required morphology of the deposit and their effect on the morphology were studied. The micro morphologies of film were studied by scanning electron microscopy and energy dispersive X-ray analysis, to get information about metal lattice parameters, texture and phase composition of the coatings which dramatically changed from to nanocrystal sheets owing to the addition of graphite oxide. The corrosion resistance properties of Zn-GO composite coatings in HCl solution were investigated by electrochemical methods. The corrosion potential - E_{corr} and corrosion current density - I_{corr} have been determined as a measure of corrosion resistance. The nanocomposite coatings obtained from optimized bath parameters, showed better corrosion protective ability and surface properties.

Keywords: Corrosion protection, Electrodeposition, Graphite oxide, Micro morphology, Nanocomposites, Scanning electron microscopy.

INTRODUCTION

The standard reversible potential zinc is -0.76 V/s standard hydrogen electrode (SHE), which is more negative than that of iron (Fe/Fe^{2+} -0.44 V/SHE). Therefore zinc is used for sacrificial cathodic protection of steel against corrosion. Nanostructured materials (1-100 nm) are known for their outstanding mechanical and physical properties due to their extremely fine grain size and high grain boundary volume fraction [1]. Significant progress has been made in various aspects of synthesis of nanoscale materials. During the last decade, extensive work on the characterization of nanocrystalline materials have been conducted. Some of the research papers in this field are of special interest because they illustrate general trends. Pulse plating is studied in order to generate nanocrystalline zinc deposits [2-5].

Electrodeposition is a versatile technique for producing nanocrystalline materials [6]. It is technologically and economically viable production route for metals, alloys and metal matrix composites, both in bulk form and as coatings. Now the focus shifting from synthesis to manufacture of useful structures and coatings having greater wear and corrosion resistance. In the metal electrodeposition, zinc can be considered as an intermediate metal, giving rise to medium values of over potentials due to secondary inhibition resulting from adsorbed hydrolized species [7]. Organic additives are studied in order to control the morphology and the properties of the deposits, eventually in combination with pulse plating [8-10]; texture and surface morphology of zinc and zinc alloys deposited on low carbon steel substrate were further investigated [11,12].

In industrial processes electrolytic plating is an alternative to hot-dip galvanizing. Both processes have advantages and disadvantages. Continual technological improvements make it difficult to conclude in favour of one process over the other. However, hot dip always includes some surface alloying by diffusion and the deposit thickness is less easily controlled than in electroplating. Electrodeposition technique can yield porous-free finished products that do not require subsequent consolidation processing. Further this process requires low initial capital and provides high production rates with few shape and size limitations [13].

In acid sulfate solutions without an organic additive, basic reproducible metallographic cross-sectional structures are obtained. In chloride electrolytes, even coarser grains are observed, because of the more activating character of chloride ions against sulfate ions [14] and despite the complex formation in solution. In cyanide baths, on the other hand, much finer grains are obtained. For continuous plating on steel sheets or wires, constant current density and rather good hydrodynamic control may be achieved over the whole cathodic surface and organic additives are not so much in use. Whatever the pH,

zinc is always more negative than hydrogen [15]. The use of additives in electrodeposition solutions is extremely important due to their influence on the growth and structure of the resulting deposits, such as grain size, brightness, internal stress, pitting and even chemical composition [16]. Properties of nano-structured electrodeposits such as hardness, wear resistance and electrical resistivity are strongly grain size dependent [17]. The grain size of the electrodeposits depends on the deposition parameters such as pH, deposition technique, current density and substrate, as well as on the type and the amount of additives included in the electrolyte [18-21].

Graphene and graphite based materials have been widely reported as support material for metal nanoparticles to obtain catalytic, optoelectronic magnetic properties, *etc*. [22,23]. Graphene is hardly electrochemically active and acts merely as a conductive host matrix for electro-active components. Thus graphene is often combined with other materials to form composites in which graphene adds conductivity while the co-material adds specific chemical or electrochemical activity. Many metal-graphene composites have been prepared [24], these usually include novel metals like gold, platinum, palladium or silver. However graphene composites incorporating more reactive base metals have not yet been reported. This would be of great interest since such composites are of significant importance for energy storage/conversion applications and for electro-catalysis.

Metal/graphene composite films have been previously prepared using simultaneous co-deposition from one-pot aqueous reaction mixture [25,26]. These involved anionic metal complexes such as $[PdCl_4]^{2-}$ or $[PtCl_6]^{2-}$. These complexes are anionic and very compatible with the anionic graphite oxide particles, but using cationic precursors such as Zn^{2+} has not yet been reported. To the best of our knowledge, no effort was paid in using graphite oxide sheets as an additive to obtain nanocrystalline zinc composites, which are expected to exhibit more excellent nano properties

In this investigation nanocrystalline zinc coating was obtained from simple acid sulphate bath. The electrodeposition of graphite oxide and cationic Zn^{2+} precursors in an aqueous one-pot mixture (both species simultaneously), resulted in the formation of composite films consisting of graphite oxide with active zinc metal. An attempt has been made to study the bath characteristics, effect of bath constituents and bath variables on the corrosion behaviour of nanocrystalline zinc-graphite oxide composite deposit.

EXPERIMENTAL

Natural graphite flakes, $ZnSO_4$, Na_2SO_4, NaCl, HCl, CTAB, H_2O_2 (30 %), $KMnO_4$ were obtained from SD Fine chemicals, India. All chemicals were of analytical reagent grade and used as received, without further purifications. The aqueous solutions were prepared in double distilled water. Natural graphite flakes were subjected to ultrasonication (Loba Life, India) in acetone for 1 h. Graphite flakes were dried well and further oxidation was carried out by Hummers and Offeman method [27].

Hull cell experiments: The standard Hull cell of 267 mL capacity was used to optimize the bath constituents and bath variables [28]. The bath parameters were optimized using a standard Hull cell. The electrodeposition process was carried out under galvanostatic condition using a regulated DC power source (Model: Acceptable Electronics, India). The cathode was mild steel panel and anode was pure zinc, copper, aluminum (99.99 %). The pH of bath solution was measured using a digital pH meter (Equipetronix, model: 7020) and adjusted with 10 % sulphuric acid or sodium bicarbonate solution. Mild steel (AISI-1079, composition C 0.5 %, Mn 0.6 %, P and S 0.05 % and rest Fe) plates of standard Hull cell size were mechanically polished using emery paper (320-800 grit size) to obtain a smooth surface and degreased by dipping in boiling trichloroethylene in degreaser plant followed by water wash. Before each experiment, the zinc anode surface was activated by dipping in 10 % HCl for few seconds followed by washing with water. The same surface area of anode and cathode was used for electrodeposition process. The bath temperature and pH were varied. The cathodic current density was controlled at 1-2 A/dm^2. Various metal nano composites were obtained by optimizing bath parameters so that a uniform, thin, film obtained on a large surface area. After electrodeposition the plates were subjected to bright dip in 1 % nitric acid for 2-3 s followed by water wash and drying. The nature and appearance of zinc deposit was carefully observed and recorded through Hull cell codes.

Galvanostatic polarization studies: The corrosion studies were carried out under galvanostatic conditions using a conventional three-electrode electrochemical cell for polarization studies with SCE reference electrode, Pt counter electrode and the electrodeposited surface as working electrode.

Microhardness test: The Vickers microhardness of deposit was determined by an indentation technique with a weight of 50 g for 10 seconds using Clemex microhardness tester, made in Japan. The average of five replicated values were recorded.

Scanning electron microscopic studies: Surface morphologies of the composite samples were examined by scanning electron microscopy, using a ZEISS Supra 40 scanning electron microscope (SEM).

EDAX analysis: The weight percentage of elements in the metal nano-composite coatings were verified by using energy dispersive X-ray analysis using FEI ESEM Quanta (EDAX) machine.

RESULTS AND DISCUSSION

Effect of various bath parameters and optimization of bath constituents: The Hull cell experiments with basic sulphate bath solution gave coarse dull deposit with pores in the current density range 1-2 A dm^{-2} at 1.7 A cell current the where as in the optimized bath it is improved to be closely packed and fine deposit. Basic bath constituents' concentrations were selected based on the appearance and uniform deposition, covering maximum surface coating and improve the nature of the deposit, which is obtained at different concentrations of all the constituents in the bath. The effect of addition agents were studied and optimized by generating composite coating from the bath solution containing different amount of graphite oxide as addition agent to the basic bath. The effect

of various Hull cell parameters are represented as shown in the Fig. 1. The bath parameters are as given in the Table-1. At this concentration, cell current and pH the deposit was uniform and almost near to a bright deposit.

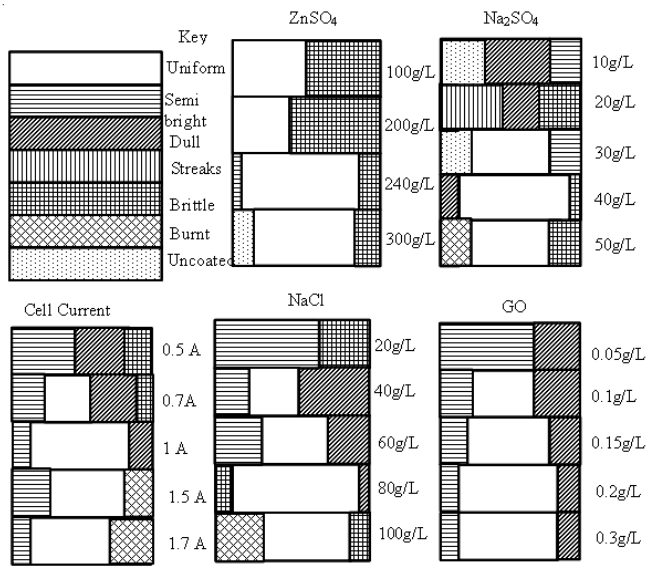

Fig. 1. Variation of Hull cell parameters for electrodeposition of Zn-GO nano composite

TABLE-1
BATH PARAMETERS FOR ELECTRODEPOSITION OF Zn-GO NANO COMPOSITE

Basic bath composition		Optimized bath composition	
$ZnSO_4$	200 g/L	$ZnSO_4$	240 g/L
Na_2SO_4	50 g/L	Na_2SO_4	40 g/L
NaCl	40 g/L	NaCl	30 g/L
CTAB	0.4 g/L	CTAB	0.4 g/L
H_3BO_3	40 g/L	H_3BO_3	40 g/L
Current	1.5 A	Current	1.0 A
–	–	Graphite oxide	0.2 g/L
Voltage	2.5 V	Voltage	2.5 V
Time	15 min	Time	10 min
pH	5	pH	7
Anode	Zinc	Anode	Zinc
Cathode	Steel	Cathode	Steel

Effect of zinc sulfate: Zinc sulphate is the main source of zinc ions in electroplating operation. There is a close relation between the concentration of zinc sulphate and appearance of plating layer in Hull cell experiment. In order to get highly corrosion resistant bright zinc deposit it is essential to strike a balance in amount of zinc sulphate in the bath solution. To find out the effect of zinc sulphate concentration on the deposit nature, zinc sulphate concentration varied from 100-300 g/L. According to the Hull cell experiment, the appropriate quantity of zinc sulphate in plating solution was 240 g/L. At this concentration the deposit was semi bright in the current density range 0.5-5 A dm^{-2}. At lower current density region uncoated and at high current density region, burnt deposits were obtained. The effect of zinc sulphate on deposit nature is shown in Fig. 1.

To increase the conductivity of the bath solution certain conducting salts having chloride and sulphate ions were added.

Effect of sodium sulfate: To find out the effect of sodium sulphate concentration on the deposit nature, concentration of sodium sulphate varied from 20-120 g/L. At a concentration of 100 g/L, the Hull cell panels were nearly bright in the current density range of 0.5-5 A dm^{-2}. Hence the concentration of sodium sulfate was fixed at 40 g L^{-1} in the bath solution. The effect of sodium sulphate on deposit nature is shown in Fig. 1.

Effect of sodium chloride: Sodium chloride was added to increase the conductance of the bath solution. The concentration of sodium chloride varied from 20-100 g L^{-1}. At low concentrations, the Hull cell panels suffered brittle and uncoated areas at low current density region. The deposit was nearly bright and large area covered over the current density range of 0.2-6 Ad m^{-2}. Further increase in the concentration (> 80 g L^{-1}) leads to burnt deposit at high current density region. The concentration of sodium chloride was fixed at 80 g L^{-1} in the bath solution (Fig. 1).

Effect of cetyltrimethyl ammonium bromide (CTAB): The concentration of CTAB varied from 0.5-2 g L^{-1}. At low concentration, the Hull cell panels suffered burnt deposit at high current density region and uncoated at lower current density region. There was no much observable difference in the nature of deposit with increase in concentration of CTAB. But yet there was a uniform, large surface area covered and a nearly bright deposit was obtained at a concentration of 1.5 g L^{-1}. The concentration of CTAB was fixed at 1.5 g L^{-1} in the bath solution.

Effect of pH and temperature: The pH of the bath solution varied from 1-7. At lower pH the specimens had uncoated areas at low current density region and burnt deposit at high current density region. At a pH 6 satisfactory deposit was obtained. At higher pH (> 5) the Hull cell panels showed burnt deposit in the high current density region. From the above observations the pH of the bath solution was kept at 5 as optimum.

Hull cell experiments showed that the optimum temperature range to get bright deposit was 293-303 K. At higher temperature (> 303 K) the supply of ions to the cathode is fastened so that bad quality of deposit is obtained. And also rate of growth of nuclei is increased, leading to coarse grained, thick deposit. Hence from the above observations the optimum deposition temperature was kept at 303 K.

Effect of cell current: There is a close relation between appearance of plating layer and cathode current density. The Hull cell experiments were carried out at different cell currents (0.5-2 A) for 10 min using optimum bath solution. At a cell current of 1 A, the deposit was uniform, semi bright and covered large surface area of the substrate current density range of 0.2-6 A dm^{-2}. At higher cell currents (> 1 A) the Hull cell cathodes covered with burnt and trees like deposit at high current density region. This was attributed to the high hydrogen discharge which leads to an increased hydroxyl ion concentration and subsequent precipitation of metal hydroxides or basic salts of the metals.

Effect of graphite oxide (GO): The concentration of graphite oxide was varied from 0.05-0.3 g L^{-1}. Graphite oxide is an amorphous state and can be easily dispersed in the aqueous medium. There are a large number of hydroxyl, carboxyl and other oxygen consisting groups in the graphite oxide structure.

Hence a small quantity of graphite oxide is incorporated in the composite coating. The expected deposit was obtained at 0.2 g L^{-1} of graphite oxide (Fig. 1).

Zn ions are proposed to adsorb on the surface of graphite oxide sheets. Therefore, nucleation sites will easily form on the surface of graphite oxide sheets and the graphite oxide sheets will migrate to adsorb on matrix owing to the effect of adsorption and mixing. Hence the introduction of graphite oxide sheets leads to a rising in nucleation site numbers which will accelerate the growth of zinc and changes the preferred orientation of the electrodeposited zinc [29].

Micro hardness: Microhardness values of composite-coated and basic bath coated samples were 145 and 130 HV, respectively. It indicates that grain size of composite-coated sample was smaller than alloy-coated sample. The higher hardness of the coating was due to the fine-grained structure of the deposit. During hardness measurements, the dispersed particles in the fine-grained matrix may obstruct the easy movement of dislocations, which was shown by higher hardness values of composite-coated samples. Thus the microhardness of the composite coatings were significantly higher in presence of graphite oxide. Increase in vickers hardness value with increased graphite oxide concentration can be attributed to better packing between the particles and improved microstructural properties of the composite samples [30]. Because of higher mechanical properties the coating surface behaviour changes and poses certain degree of resistance to corrosion and surface deterioration.

Surface morphology by SEM and EDX analysis: Zn-GO composite coating is deposited on the SS surface with the variable bath parameters. Graphite oxide was added to basic bath along with sonication to ensure a smart dispersion of graphene particles inside zinc matrix on SS. The morphological characterization of prepared samples was done using a scanning electron microscope as shown in Fig. 2. In Fig. 2(A), it can be seen that, porous, net like structures are observed for the composite deposition from basic bath. The addition of graphite oxide leads to surface associated with crystal growth and occupies the grain boundaries. In case of the composite obtained from optimized bath as seen in the Fig. 2(B), the SEM image clearly indicates the presence of graphite oxide flakes and visible in the inset image. Hence SEM study suggests proper bonding between matrix and reinforcement along their interface.

The morphology of Zn-GO composites film changes significantly with high roughness. This dramatic change in morphology is certainly caused by the introduction of graphite oxide. Although the graphite is a non-load bearing constituent, a strong particle/matrix interface helps graphite particles embed themselves into the matrix properly, improving the fracture resistance. The particles are well embedded in the matrix and the fracture shows ductile behaviour as river patterns are quite prominent. The introduction of graphite oxide sheets lead to a raise in nucleation sites number which will accelerate the growth of zinc and changes the preferred orientation of the electrodeposited Zn [31].

Fig. 3 and Table-2 show the EDS spectra and the quantitative elementary analysis of Zn-GO composite coating obtained from the optimized bath respectively. The EDS spectrum indicates that a strong particle/matrix interface helps graphite oxide particles embed themselves into the matrix properly in the composites because of the presence of carbon and oxygen

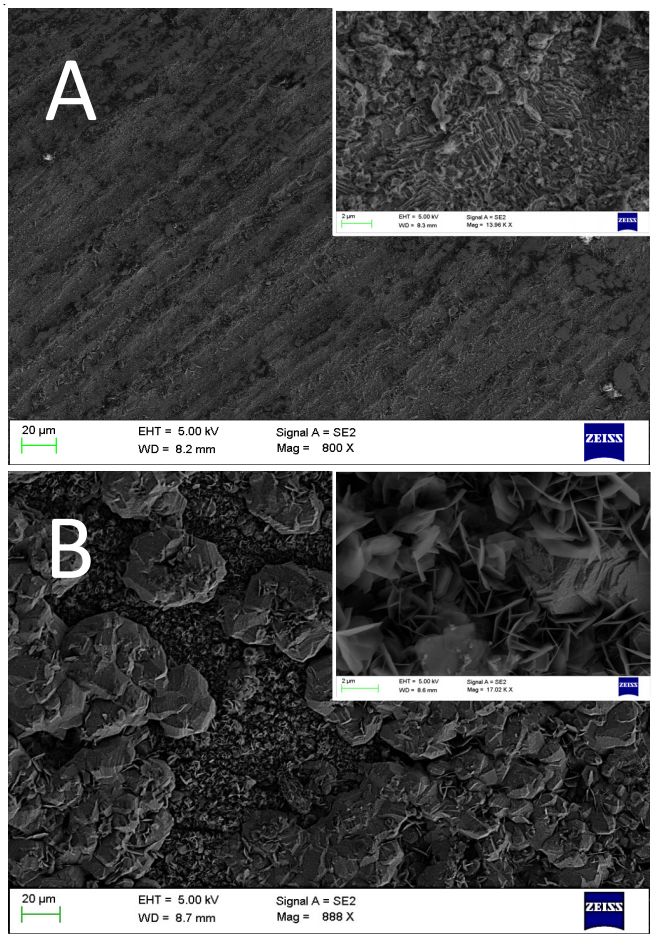

Fig. 2. SEM images of (A) Zn (B) Zn-GO nano composite coatings on stainless steel from basic bath and optimized bath respectively. The insets are the corresponding high-resolution images

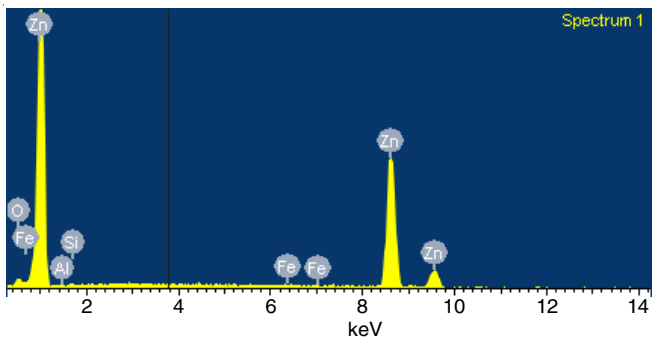

Fig. 3. EDS spectrum of Zn-GO nano composite coatings on stainless steel from optimized bath

TABLE-2
QUANTITATIVE ELEMENTARY ANALYSIS (EDAX)
OF Zn-GO NANO COMPOSITE COATINGS

Element	Weight (%)	Atomic (%)
O K	4.40	15.83
C K	5.00	6.00
Fe K	0.00	0.00
Zn L	88.60	78.17

TABLE-3
CORROSION PARAMETERS OF Zn-GO NANO COMPOSITE COATINGS IN HCl OF DIFFERENT CONCENTRATIONS

Electroplating bath	Corrosion medium					
	0.05 N HCl		0.1 N HCl		0.2 N HCl	
	E_{corr} (V)	I_{corr} (mA cm^{-2})	E_{corr} (V)	I_{corr} (mA cm^{-2})	E_{corr} (V)	I_{corr} (mA cm^{-2})
Basic	1.02	2.5	1.02	2.8	1.02	3.7
Optimized	1.03	0.5	1.02	0.7	1.05	1.1

as shown in the Table-2. From the Fig. 3, it can be seen that a region in steel is covered with-88 % of zinc sample. Distinct zinc, carbon and oxygen peaks can be seen from the EDS spectra. Hence there is an improvement in interfacial bonding between the graphite zinc on steel substrate [32].

Electrochemical corrosion studies: The electrochemical polarization measurements were carried out under galvanostatic conditions in 0.05, 0.1 and 0.2 HCl solution to study the corrosion behaviour of the surface nano composite coatings which were generated on stainless steel from the basic and optimized bath. The galvanostatic polarization curves obtained from 0.2N HCl for the steel samples coated with nano composites from basic bath and optimized bath are shown in Fig. 4.

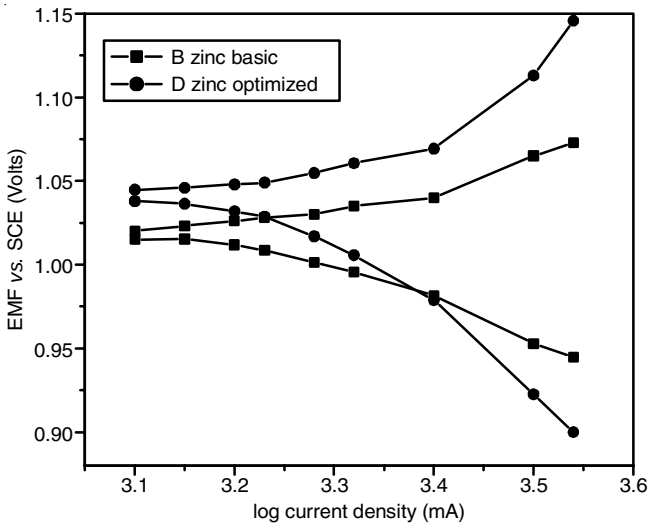

Fig. 4. Galvanostatic polarization curves in 0.2 N HCl for Zn-GO nano composite coatings on stainless steel from (A) basic bath and (B) optimized bath

In order to study the effect of graphite oxide content on the corrosion behaviour of stainless steel, galvanostatic polarization was carried out with electrode immersion in 0.05, 0.1 and 0.2 N HCl solution. The extent of corrosion protection by this composite coating was obtained from Tafel plots. There is no much shift in the polarization curves either towards positive or negative potentials in case of composite-coated samples from the optimized bath when compared to that of basic bath as shown in Fig. 4.

The value of I_{corr} reduced from 3.7 mA cm^{-2} to 1.1 mA cm^{-2} for optimized bath. This may be attributed to the good wettability and chemical compatibility between the matrix and graphite oxide [33]. The improved corrosion protection in the presence of graphite oxide can be explained by two mechanisms of the nanocomposite coatings. First, the graphite oxide nanoparticles act as inert physical barriers by occupying very small pores in the metal matrix, which modifies the Zn layer microstructure and provides a superior corrosion resistance of the composite coating in comparison with the pure alloy coating [34].

With increase in acid concentration the corrosion resistance is little decreased, may be due to the insertion of the acid into the pores of the coating. The corrosion parameters are given in the Table-3. The improved corrosion protection in the presence of graphite oxide may be due to the reduced hydrogen reduction process and the corrosion rate [35]. Also surface passivation can occur due to formation of firmly bonded, hard and non-porous layer. The degree of passivation will depend on the acidity of the environment.

Conclusion

A nanocrystalline zinc-GO was electrodeposited on mild steel from simple acid sulphate bath. The technique adopted to obtain the Zn-GO composite is a versatile technique and is a technologically and economically viable production route to metals, alloys and metal matrix composites, both in bulk form and as coatings. The obtained composite coatings by varying the bath parameters, showed improved surface mechanical properties. The deposits obtained from optimum bath are highly corrosion resistant as it was evident by SEM and electrochemical studies. The higher corrosion resistance could be attributed to the presence of graphite oxide in the composite matrix.

REFERENCES

1. H.S. Nalwa, Handbook of Nanostructured Materials and Nanotechnology, vol. 1, p. 1 (2000).
2. K. Saber, C.C. Koch and P.S. Fedkiw, *Mater. Sci. Eng. A*, **341**, 174 (2003); https://doi.org/10.1016/S0921-5093(02)00198-3.
3. K.M. Youssef, C.C. Koch and P.S. Fedkiw, *Electrochim. Acta*, **54**, 677 (2008); https://doi.org/10.1016/j.electacta.2008.07.048.
4. D.L. Wang, Y.Q. Wu, X.Y. Zhong, W.Q. Zhang, M.C. Li and J.N. Shen, *Russ. J. Electrochem.*, **45**, 291 (2009); https://doi.org/10.1134/S1023193509030082.
5. M.S. Chandrasekar, S. Srinivasan and M. Pushpavanam, *J. Mater. Sci.*, **45**, 1160 (2010); https://doi.org/10.1007/s10853-009-4045-z.
6. F. Ebrahimi and D. Kong, T.E. Mattehews and Q. Zhai, Processing and Fabrication of Advanced Materials, edn 7, p. 509 (1998).
7. H. Fischer, Elektrolytische Abscheidung und Elektrokristallisation von Metallen, pp. 618–623 (1954).
8. A. Gomes and M.I. da Silva Pereira, *Electrochim. Acta*, **51**, 1342 (2006); https://doi.org/10.1016/j.electacta.2005.06.023.
9. M. Mouanga, L. Ricq, G. Douglade, J. Douglade and P. Ber¸cot, *Surf. Coat. Tech.*, **201**, 762 (2006); https://doi.org/10.1016/j.surfcoat.2005.12.036.
10. J.C. Ballesteros, P. Díaz-Arista, Y. Meas, R. Ortega and G. Trejo, *Electrochim. Acta*, **52**, 3686 (2007); https://doi.org/10.1016/j.electacta.2006.10.042.
11. M.Ch. Li, L.L. Jiang, W.Q. Zhang, Y.H. Qian, S.Z. Luo and J.N. Shen, *J. Solid State Electrochem.*, **11**, 549 (2007); https://doi.org/10.1007/s10008-006-0194-z.

12. M. Mouanga, L. Ricq, L. Ismaili, B. Refouvelet and P. Berçot, *Surf. Coat. Technol.*, **201**, 7143 (2007); https://doi.org/10.1016/j.surfcoat.2007.01.022.
13. C. Cheung, D. Wood and U. Erb, in eds.: C. Suryanarayana, J. Singh and F.H. Froes Proceesing and Properties of Nanocrystalline Materials, TMS Publication, Warrendale, PA, pp. 479-484 (1996).
14. A.T. Vagramyan and M.A. Zhamagortsyants, Electrodeposition of Metals and Inhibiting Adsorption, Translation from Russian, U.S. Dept. of Commerce, NTIS, Springfield, VA, Contract NSF, C-466, p. 40 (1974).
15. M. Pourbaix, Atlas d'equilibreselectrochimiques, Gauthier-Villars, Paris, pp. 409 (1963).
16. T.V. Venkatesha, J. Balachandra, S.M. Mayanna and R.P. Dampal, *Met. Finish.*, **84**, 29 (1986).
17. F. Ebrahimi and H.Q. Li, *Rev. Adv. Mater. Sci.*, **5**, 134 (2003).
18. F. Ebrahimi, G.R. Bourne, M.S. Kelly and T.E. Matthews, *Nanostruct. Mater.*, **11**, 343 (1999); https://doi.org/10.1016/S0965-9773(99)00050-1.
19. K.L. Morgan, Z. Ahmed and F. Ebrahimi, *MRS Proceeding*, B.**3**.11.1, 634 (2001).
20. F. Ebrahimi and Z. Ahmed, *Mater. Charact.*, **49**, 373 (2002); https://doi.org/10.1016/S1044-5803(02)00305-4.
21. A.M. El-Sherik and U. Erb, *J. Mater. Sci.*, **30**, 5743 (1995); https://doi.org/10.1007/BF00356715.
22. Y.K. Kim, H.K. Na and D.H. Min, *Langmuir*, **26**, 13065 (2010); https://doi.org/10.1021/la102372z.
23. Q. Xiang, J. Yu and M. Jaroniec, *Chem. Soc. Rev.*, **41**, 782 (2012); https://doi.org/10.1039/C1CS15172J.
24. Q. Xiang, J. Yu and M. Jaroniec, *J. Am. Chem. Soc.*, **134**, 6575 (2012); https://doi.org/10.1021/ja302846n.
25. C. Liu, K. Wang, S. Luo, Y. Tang and L. Chen, *Small*, **7**, 1203 (2011); https://doi.org/10.1002/smll.201002340.
26. Y.G. Zhou, J.J. Chen, F.-B. Wang, Z.H. Sheng and X.H. Xia, *Chem. Commun.*, **46**, 5951 (2010); https://doi.org/10.1039/c0cc00394h.
27. W.S. Hummers Jr. and R.E. Offeman, *J. Am. Chem. Soc.*, **80**, 1339 (1958); https://doi.org/10.1021/ja01539a017.
28. D. Pletcher and F.C. Walsh, Industrial Electrochemistry, Chapman and Hall, New York, edn 2, pp. 389-390 (1990).
29. W. Lv, D.M. Tang, Y.B. He, C.H. You, Z.Q. Shi, X.C. Chen, C.M. Chen, P.X. Hou, C. Liu and Q.H. Yang, *ACS Nano*, **3**, 3730 (2009); https://doi.org/10.1021/nn900933u.
30. P. Garg, P. Gupta, D. Kumar and O. Parkash, *J. Mater. Environ. Sci.*, **7**, 1461 (2016).
31. W. He, L. Zhu, H. Nan, H. Liu and W. Li, *Int. J. Mater. Sci. Eng.*, **1**, 32 (2013).
32. Berman, A. Erdemir and A.V. Sumant, *Carbon*, **59**, 167 (2013); https://doi.org/10.1016/j.carbon.2013.03.006.
33. K.E. Wise, C. Park, E.J. Siochi and J.S. Harrison, *Chem. Phys. Lett.*, **391**, 207 (2004); https://doi.org/10.1016/j.cplett.2004.04.096.
34. K. Vathsala, T.V. Venkatesha, B.M. Praveen and K.O. Nayana, *Eng.*, **2**, 580 (2010); https://doi.org/10.4236/eng.2010.28074.
35. B.M. Praveen and T.V. Venkatesha, *Int. J. Electrochem.*, **Article ID 261407** (2011); https://doi.org/10.4061/2011/261407.